Scleraxis-Lineage Cell Depletion Improves Tendon Healing

Authors: Katherine T. Best[1], Keshia E. Mora[1,2], Emma Knapp[1], Mark R. Buckley[1,2], Alayna E. Loiselle[1*]

Affiliations

[1]Center for Musculoskeletal Research, University of Rochester Medical Center, Rochester, NY 14642, United States of America

[2]Department of Biomedical Engineering, University of Rochester, Rochester, New York, United States of America.

***Corresponding author**

Alayna E. Loiselle, PhD

Center for Musculoskeletal Research

University of Rochester Medical Center

601 Elmwood Ave

Box 665

Rochester, NY

14642

Phone: 585-275-7239

Fax: 585-276-2177

Alayna_Loiselle@urmc.rochester.edu

Conflict of Interest Statement: The authors have declared that no conflict of interest exists.

Abstract

Despite the requirement for *Scleraxis*-lineage (Scx^{Lin}) cells during tendon development, the function of Scx^{Lin} cells during adult tendon repair, post-natal growth, and adult homeostasis have not been defined. Therefore, we crossed Scx-Cre and Diphtheria Toxin Receptor (DTR) mouse models to inducibly deplete Scx^{Lin} cells prior to acute flexor tendon injury and repair ($ScxLin^{DTR}$) and hypothesized that $ScxLin^{DTR}$ mice would exhibit worse healing than wildtype littermates. Surprisingly, depletion of Scx^{Lin} cells resulted in increased biomechanical properties without detriments to tendon gliding function at 28 days post-repair, indicative of regeneration. These improvements in biomechanical properties correspond to increased αSMA+ myofibroblasts in $ScxLin^{DTR}$ repairs, indicating that increased myofibroblast-mediated matrix remodeling may be responsible for accelerated recovery of tensile strength. Furthermore, we have defined the relative timing of Scx^{Lin} cell localization relative to collagen deposition in bridging tissue of the repair and demonstrated a predominance of non-Scx^{Lin} cells in the early bridging tissue, consistent with lack of bridging tissue disruption in $ScxLin^{DTR}$ repairs. Lastly, we utilized $ScxLin^{DTR}$ mice to assess effects of tendon cell depletion on post-natal tendon growth and adult tendon homeostasis. Collectively, these findings enhance our understanding of tendon cell localization, function, and fate during healing, growth, and homeostasis.

Introduction:

Despite the significant efforts toward improving tendon healing and regeneration, the specific cellular contributions during tendon healing have not been extensively characterized(1). While many studies have examined the potential of using various stem cell populations to promote healing, originating from both tendon intrinsic(2) and extrinsic sources(3), little focus has been directed toward defining the functions and therapeutic potential of tendon cells during tendon healing following an acute injury. Tendon cells are increasingly being recognized as a heterogenous population of cells where many, but not all, express the gene *Scleraxis* (*Scx*)(4-6). Understanding the localization and function of tendon cell subpopulations during healing could be instrumental in discovering why tendon heals using scar-mediated processes, resulting in poor patient outcomes, and could be used to develop pro-regenerative approaches to improve healing.

Scx, a basic helix-loop-helix transcription factor, is currently the most well-characterized marker that the field possesses to study tendon(7). *Scx* has been utilized to examine tendon biology and development(8-10), healing and regeneration(4, 11-13), differentiation(14-17), and mechano-transduction(18, 19). Functionally, *Scx* expression has previously been shown to drive matrix production and remodeling(11, 20, 21), epithelial-to-mesenchymal transition(22), development of force-transmitting tendons(8), and effect focal adhesion morphology(19). Despite the effort to understand the functions of *Scx* as a transcription factor, the function and requirement of *Scx*-lineage (Scx^{Lin}) cells in tendon repair, post-natal growth and homeostasis has not been defined.

Previous studies examining the localization and role of tendon cells during healing are limited. *Scx*-GFP mice(23) have been used to visualize tendon cells in many studies; however, previous work has suggested that extrinsic, paratenon-derived *Scx*-GFP^- cells can turn on *Scx* expression and become *Scx*-GFP^+ by 14 days post-Patellar tendon injury(13). This makes interpretation using *Scx*-GFP mice complicated during *in vivo* studies as it becomes difficult to determine if a *Scx*-GFP^+ cell is tendon-derived or simply activating *Scx* expression post-injury. Other studies have utilized the inducible Scx-Cre^{ERT2} mouse to label Scx^+ cells prior to injury to allow tracking of these cells post-injury (Scx^{Ai9}). Howell *et al*. determined that while *Scx*-GFP cells and Scx^{Ai9} tendon

cells localized to the regenerated tendon in neonatal mice, these cells were not recruited to the scar tissue/bridging tissue during adult healing in Achilles tendon(12). In contrast, we have previously demonstrated that Scx^{Ai9} tendon cells organize into a linear, cellular bridge spanning the scar tissue between the tendon stubs following acute injury and repair of the flexor digitorum longus tendon(4). While these studies suggest that tendon and injury model-specific differences may modulate the Scx^{Lin} cell contribution to injury, it also highlights the near complete lack of characterization of Scx^{Lin} cell function in the healing process.

In the present study, we hypothesized that Scx^{Lin} tendon cells would be required for healing in a model of acute flexor tendon repair by driving formation of a collagenous tissue bridge. We utilized a genetic mouse model of Scx^{Lin} cell depletion to directly assess the function of tendon cells during healing and surprisingly discovered that depletion of Scx^{Lin} tendon cells resulted in improved tendon biomechanical properties. We also examined the relationship between bridging tendon cells and bridging collagen matrix, tendon cell proliferation throughout healing, the differentiation potential of tendon cells to become myofibroblasts during late stages of healing, and the effects of Scx^{Lin} cell depletion on tendon post-natal growth and homeostasis.

Results:

Successful ablation of *Scleraxis*-lineage tendon cells using diphtheria toxin receptor mouse model.

Scx^{Lin} cells account for ~80% of tendon cells in the flexor digitorum longus (FDL) tendon (Fig. 1A and B). To deplete tendon cells, Scx-Cre mice were crossed to diphtheria toxin receptor ($DTR^{F/F}$) animals ($ScxLin^{DTR}$) (Fig. 1C). Five local injections of DT (Fig. 1D) resulted in 57% depletion of tendon cells in uninjured $ScxLin^{DTR}$ FDL tendons relative to WT control littermates ($p < 0.0001$) (Fig. 1E and F). Tendon cell number was unaffected in the contralateral FDL, indicating that local DT injections did not induce cell death in locations other than the targeted hindpaw (Fig. 1E and F). $ScxLin^{DTR}$ tendons exhibited a small number of apoptotic cells peripheral to, but not within, the tendon suggesting that a 10-day DT washout period was sufficient for all tendon-specific DT-induced cell death to occur (Fig. S1A). Both $ScxLin^{DTR}$ and WT littermates exhibited PCNA+ cells within the muscle, but not within then tendon, and $ScxLin^{DTR}$ exhibited a few PCNA+ cells within the tendon that were not present in WTs (Fig. S1B). $ScxLin^{DTR}$ tendons exhibited more F4/80+ macrophages peripheral to the tendon, potentially due to macrophage recruitment to the tendon to clean up apoptotic cell debris (Fig. S1C).

Ablation of Scleraxis-lineage cells results in significantly increased biomechanical properties by day 28 post repair while not affecting gliding function.

To define the functional effects of Scx^{Lin} cell depletion on tendon healing, mice received five DT injections to deplete Scx^{Lin} cells followed by FDL repair 10 days following the final injection (Fig. 2A). $ScxLin^{DTR}$ repairs were trending towards increased MTP range of motion at day 14 relative to WT littermates (WT vs $ScxLin^{DTR}$, $p = 0.0711$), but this trend was absent by day 28 post-repair (Fig. 2B). $ScxLin^{DTR}$ healing tendons did not significantly differ in gliding resistance at either day 14 or 28 post-repair (Fig. 2C). While biomechanical properties were not altered between groups at day 14, both stiffness and maximum load at failure were significantly increased in $ScxLin^{DTR}$ healing tendons relative to wildtype littermates at day 28 post-repair (Stiffness: WT: 6.48 ± 0.75, $ScxLin^{DTR}$: 11.22 ± 1.83 , $p = 0.0237$; Maximum load at failure: WT: 1.54 ± 0.17,

ScxLin^{DTR}: 2.44 $\pm$ 0.24 , p = 0.0061) (Fig. 2D and E). Between days 14 and 28, WT tendon stiffness increased by 39.06% while ScxLin^{DTR} stiffness increased by 109.33%, and WT tendon maximum load at failure increased by 52.48% while ScxLin^{DTR} maximum load at failure increased by 162.37%, indicating that ScxLin^{DTR} repairs heal at an accelerated rate relative to wildtype littermates.

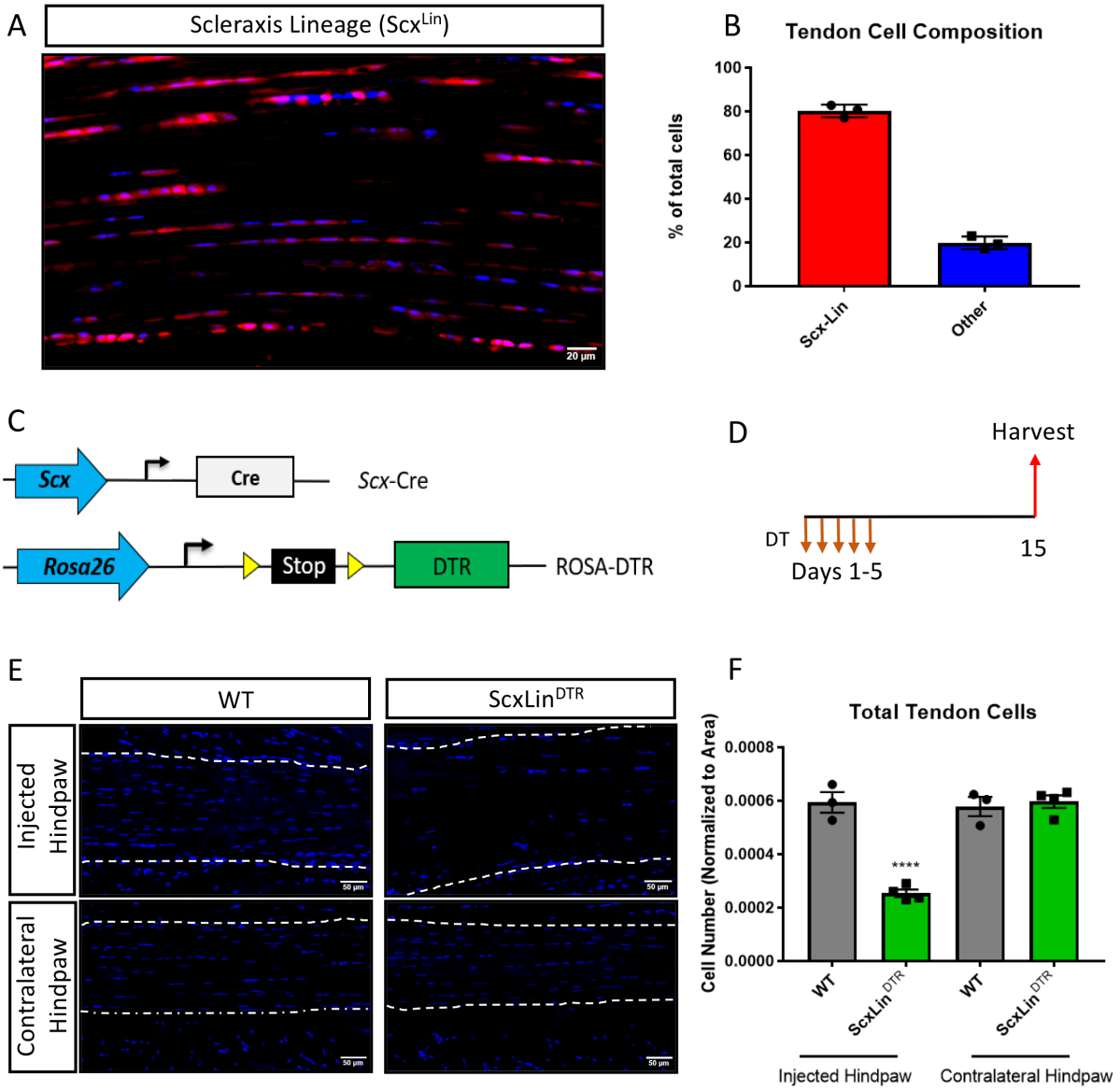

Figure 1. Model of Scleraxis lineage tendon cell depletion. Scx-Cre mice were crossed to ROSA-Ai9 reporter to trace (A) and quantify (B) *Scx* lineage cells (Scx^{Lin}) in uninjured flexor tendon. N=3. To deplete Scx^{Lin}, Scx-Cre mice were crossed to the diphtheria toxin receptor mouse (ScxLin^{DTR}, C). Mice received five hindpaw injections of DT and were harvested ten days after the final injection (D). Hindpaw sections from both WT and ScxLin^{DTR} injected hindpaws contralateral hindpaws (E). Quantification of injured and contralateral hindpaw tendon cell number (F). When needed, tendon outlined by white dotted line. Nuclei stained with DAPI. N=3-4 per genotype. 2-way ANOVA with Sidak's multiple comparisons test used to assess statistical significance of tendon cell ablation between hindpaw (injected with DT or contralateral) and genotype (WT and ScxLin^{DTR}). **** indicates p<0.0001 relative to all other groups.

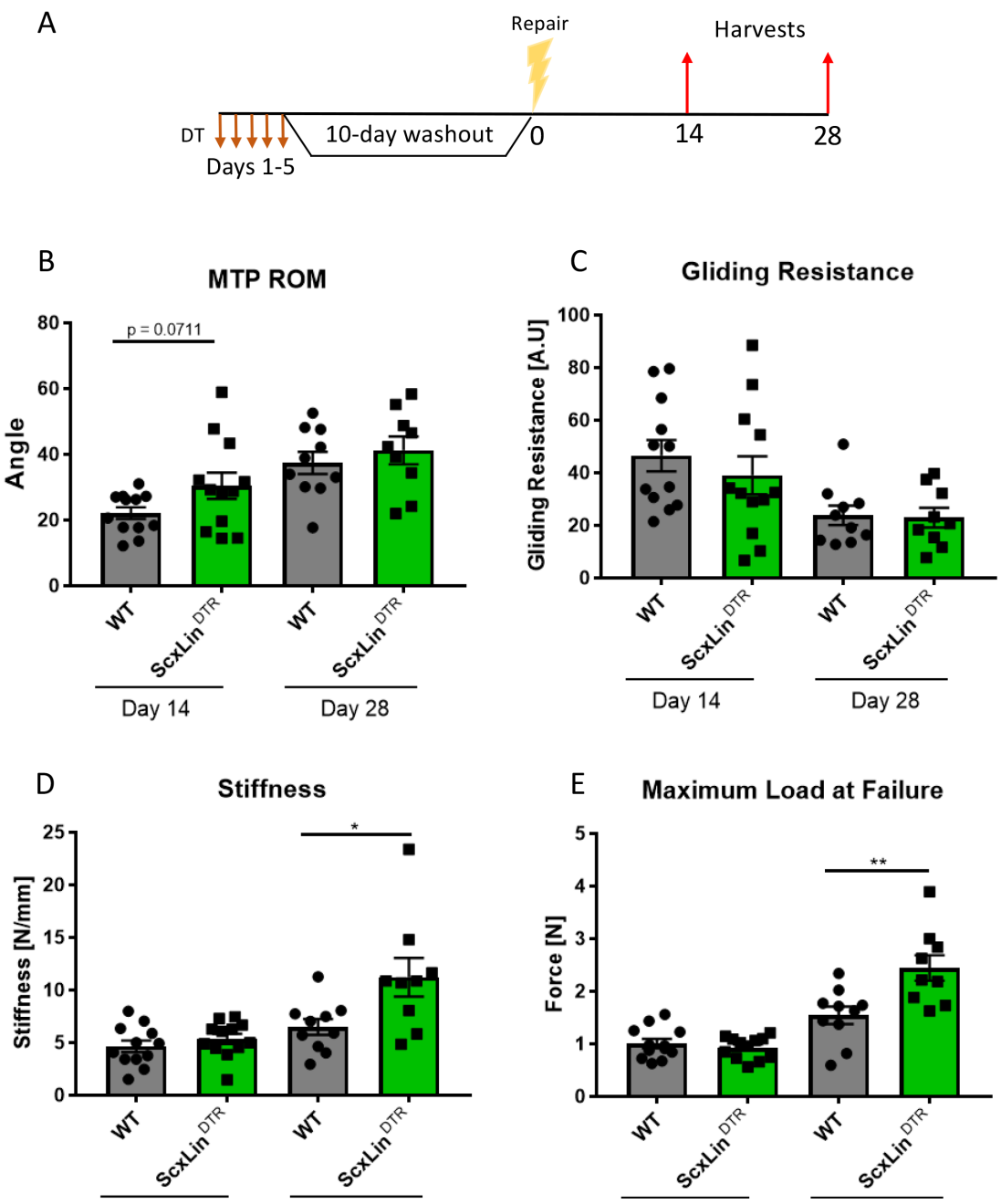

Figure 2. ScxLin^{DTR} tendons heal with significantly increased biomechanical properties. Mice received five hindpaw injections of DT on consecutive days, underwent flexor tendon repair surgery ten days after the final DT injection, and were harvested at 14 and 28 days post-repair (A). Measurement of metatarsophalangeal (MTP) joint flexion angle (B), gliding resistance (C), stiffness (D), and maximum load at failure (E) of WT and ScxLin^{DTR} repaired tendons. N=9-12 per genotype per timepoint. Students t-test used to assess statistical significance between genotypes at a given timepoint. * indicative of $p < 0.05$, ** indicative of $p < 0.01$.

Scleraxis-lineage cells are not required for the formation of a bridging collagen matrix during tendon healing.

We have previously demonstrated that bridging tendon cells correspond to a region of bridging collagen matrix in the scar tissue(4). While there were no apparent differences in tissue morphology between groups at days 14 or 28 post-repair (Fig. 3B), we wanted to determine if tendon cell depletion prevented formation of the bridging collagen. Masson's trichrome staining revealed presence of bridging collagen through the scar in both groups at days 14 and 28, indicating that depletion of Scx^{Lin} tendon cells does not prevent formation of the bridging collagen matrix (Fig. 3C).

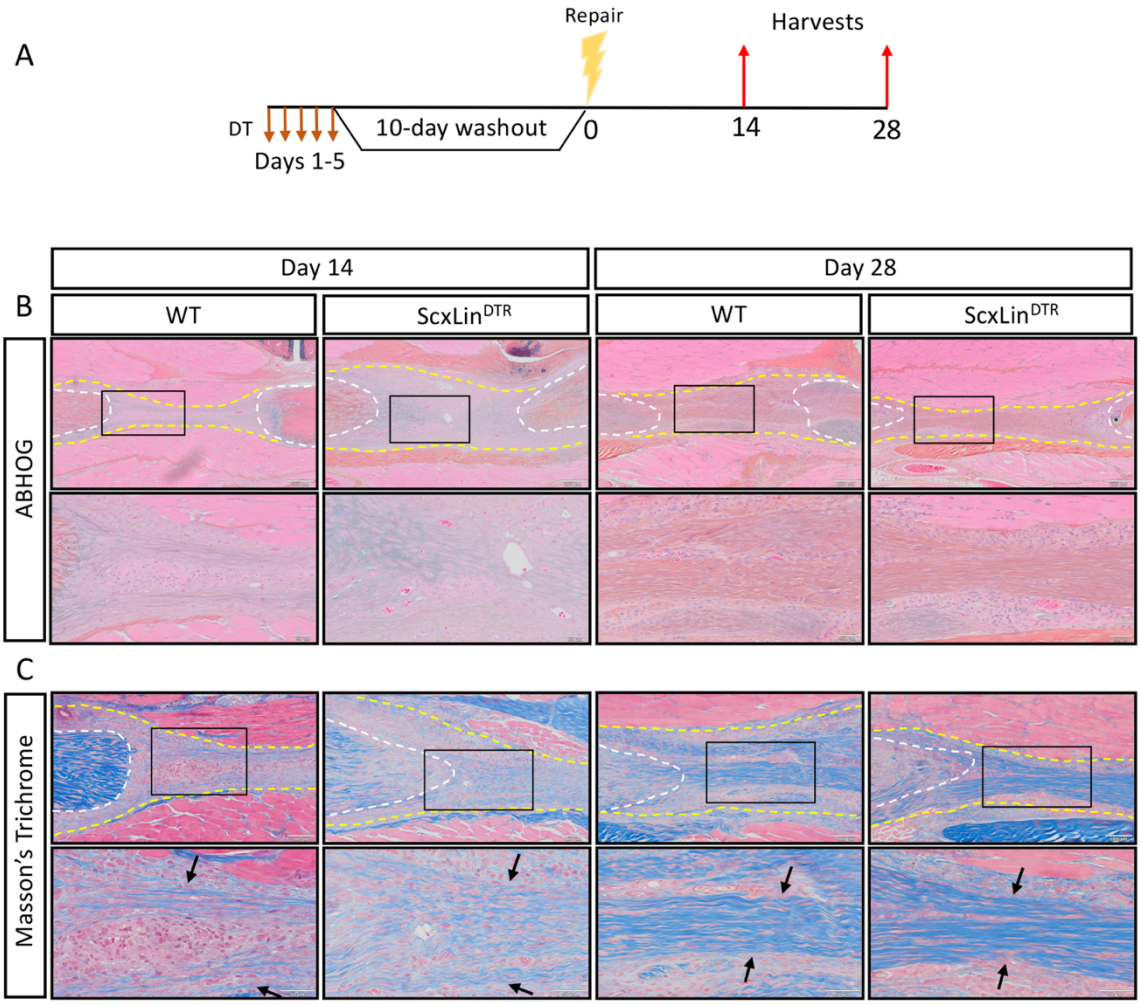

Figure 3. Scx^{Lin} cell depletion does not disrupt formation of a bridging collagen matrix. Mice received five hindpaw injections of DT on consecutive days, underwent flexor tendon repair surgery ten days after the final DT injection, and were harvested at 14 and 28 days post-repair (A). Alcian blue/hematoxylin and Orange G stain utilized to assess overall morphology (B). Masson's trichrome stain used to visualize collagen content and organization (C). Tendon is outlined by white dotted line and scar tissue by yellow dotted line. Black boxes indicate location of higher magnification images. Boundaries of bridging collagen indicated by black arrows. N=4 genotype per timepoint. Suture indicated by *.

Scx^{Lin} Depletion enhances myofibroblast content during tendon healing.

We have previously demonstrated that elevated F4/80+ macrophages and αSMA+ myofibroblasts are associated with increased tendon maximum load at failure(24). No significant differences in F4/80+ macrophages were detected between genotypes at either day 14 or 28 post-repair (Fig. 4B). While αSMA+ myofibroblasts were not significantly altered at day 14 (D14: WT vs DTR, $p = 0.3790$), $ScxLin^{DTR}$ healing tendons had significantly increased levels of αSMA+ myofibroblasts relative to wildtype littermates at D28 ($p = 0.0188$) (Fig. 4C). We have previously demonstrated that S100a4 is an important molecule that can influence tendon biomechanical properties and gliding function during flexor tendon healing(25). No differences in S100a4+ cells were observed in $ScxLin^{DTR}$, relative to WT at either day 14 or 28 post-repair (Fig. 4D). Thus, αSMA+ myofibroblasts are the most likely contributor to the increased biomechanical properties seen in $ScxLin^{DTR}$ healing tendon. However, little is understood about the varied functions and sources of αSMA+ myofibroblasts during tendon healing.

Tendon cells do not differentiate into myofibroblast by day 28 post-repair.

We have previously reported that while many Scx^{Ai9} tendon cells residing within the tendon stubs during healing differentiate into αSMA+ expressing myofibroblasts, the majority of bridging Scx^{Ai9} tendon cells do not differentiate into myofibroblasts by 14 days post-repair in mouse flexor tendons(4). To assess if bridging tendon cells differentiate into αSMA+ myofibroblasts during later stages of healing, co-immunofluorescence of tdTomato (labels Scx^{Ai9} cells) and αSMA was performed. While tendon cells in the stubs continued to express αSMA, bridging tendon cells had still not differentiated into myofibroblasts by 21 or 28 days post-repair (Fig. 5B and C). It has previously been demonstrated that approximately 65% of αSMA-lineage cells express *Scx* at day 14 post-injury in patellar tendon. To confirm that actively expressing αSMA+ myofibroblasts express *Scx* post-injury, $Scx\text{-}Cre^{ERT2}$; $ROSA\text{-}Ai9^{F/F}$ mice were injected with TAM on days 10-12 post-repair to label cells expressing *Scx* near the time of a day 14 harvest ($Scx^{10\text{-}12}$) (Fig. 5D). Essentially all αSMA+ myofibroblasts

express *Scx* by day 14 post-flexor tendon repair (Fig. 5E), suggesting that *Scx* expressing myofibroblasts in the bridging region are not derived from Scx^{Ai9} cells that are labelled in the adult tendon prior to injury.

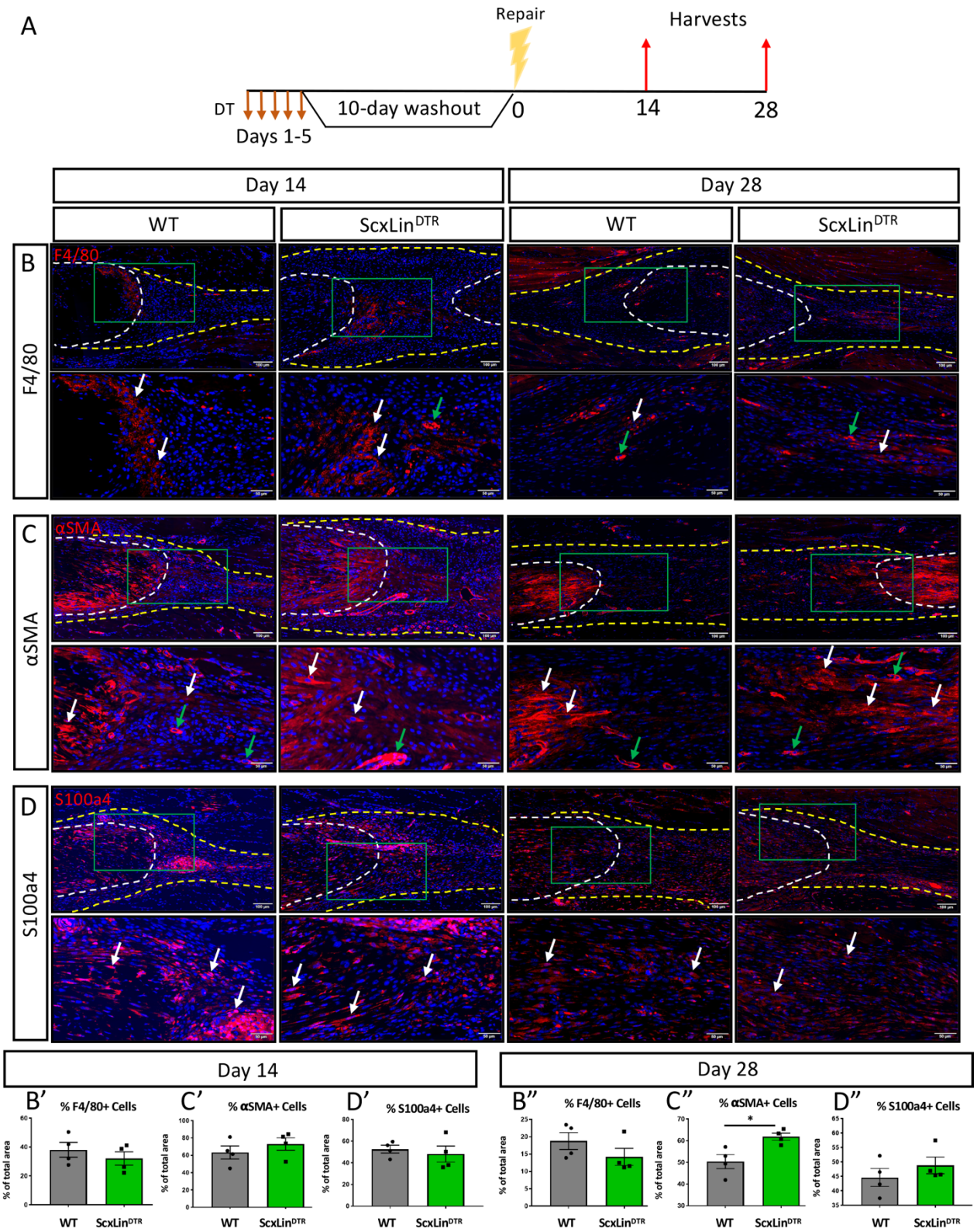

Figure 4. ScxLin^{DTR} repaired tendons heal with increased presence of αSMA+ myofibroblasts. Mice received five hindpaw injections of DT on consecutive days, underwent flexor tendon repair surgery ten days after the final DT injection, and were harvested at 14 and 28 days post-repair (A). Immunofluorescence of WT and ScxLin^{DTR} repair tendons 14 and 28-days post-repair to assess F4/80+ macrophages (B), αSMA+ myofibroblasts (C), and S100a4+ cells (D). Tendon is outlined by white dotted line and scar tissue by yellow dotted line. Purple boxes indicate location of higher magnification images. Examples of positive stain indicated by white arrows, while examples of auto-fluorescent blood cells and α-SMA+ blood vessels indicated by green arrows. Quantification of F4/80 (A' & A''), αSMA (B' & B''), and S100a4 (C' & C'') fluorescence. N=4 per genotype per timepoint. Student's t-test used to assess statistical significance between genotypes at a given timepoint, except for D28 F4/80 and S100a4 which required a Mann-Whitney test. * indicates $p < 0.05$.

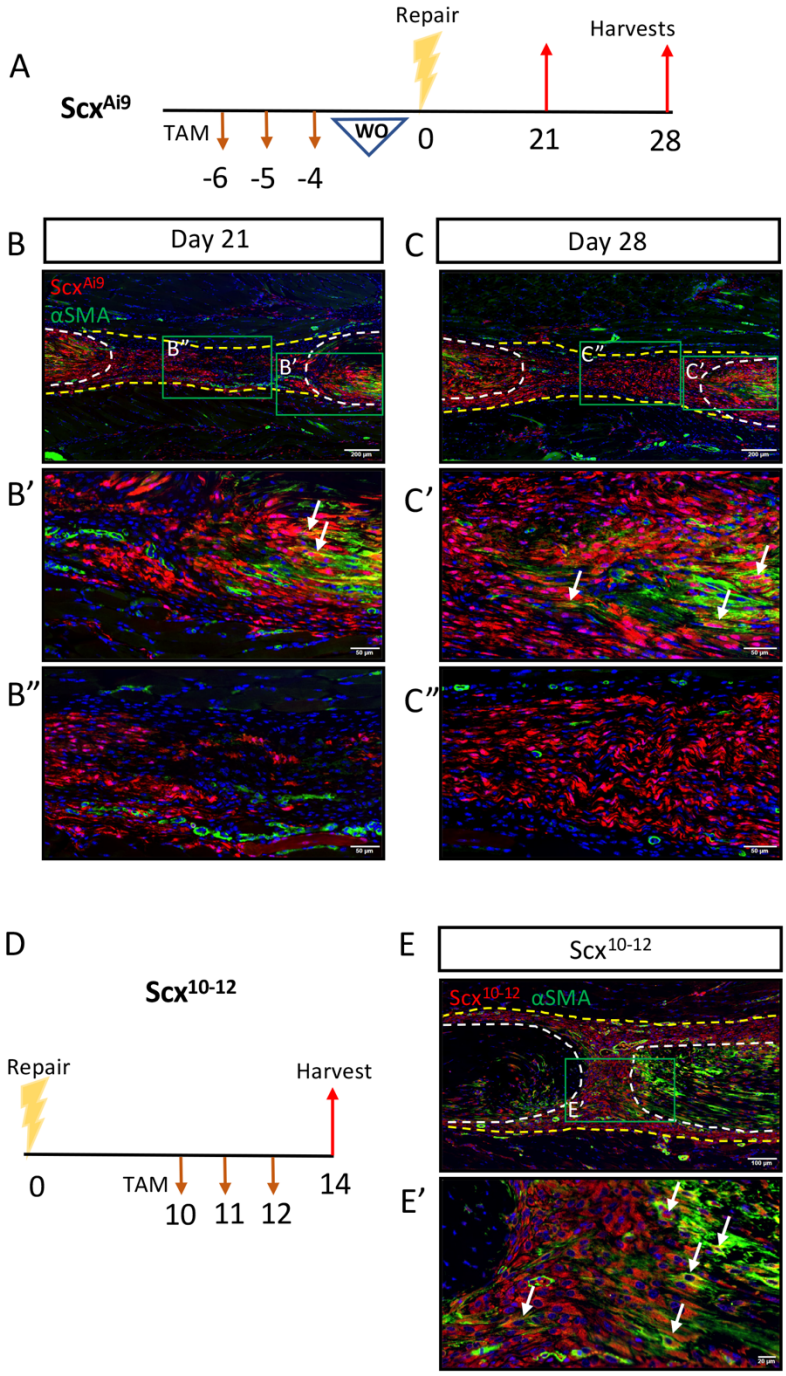

Figure 5. Bridging Scx^{Ai9} mice do not differentiate into αSMA+ myofibroblasts. Scx^{Ai9} mice were injected with TAM for three days, allowed to WO for four days prior to repair surgery, and were harvested at days 21 and 28 post-repair (A). Co-immunofluorescence between Scx^{Ai9} (red) and αSMA+ myofibroblasts (green) at 21 (B) and 28 (C) days post-repair. Green boxes indicate location of higher magnification images (B' & C': tendon stub, B'' & C'': bridging tissue). Scx^{Ai9} mice were injected with TAM on days 10-12 and harvested on day 14 to label cells actively expressing *Scx* during healing (Scx$^{10-12}$) (D). Co-immunofluorescence between Scx$^{10-12}$ (red) and αSMA+ myofibroblasts (green) (E). Green box indicates location of higher magnification (E': includes both stub and scar regions). Examples of co-localization indicated by white arrows. Nuclei stained with DAPI. Tendon is outlined by white dotted lines and scar tissue by yellow dotted lines. N=3-4 per timepoint.

Robust tendon cell bridging is first detected at day 10 post-repair and corresponds to organized collagen matrix in the scar.

We have previously demonstrated that Scx^{Ai9} tendon cells bridge the injury site by 14 days post-repair and these bridging Scx^{Ai9} cells correspond to a bridging, linear collagen matrix in the scar(4), and have established that depletion of Scx^{Lin} cells does not disrupt formation of this collagenous bridge (Fig. 3). However, further exploration of the timing of collagen formation and bridging Scx^{Ai9} could be informative as to Scx^{Ai9} cell function. Scx^{Ai9} cells are not found in the scar at day 7 post-repair, indicating the cellular bridge forms between days 7 and 14 post-repair(4). To determine when Scx^{Ai9} cells first bridge the injury site and how this compares to development of bridging collagen matrix, Scx^{Ai9} mice were harvested at 8, 10, and 12 days post-repair and assessed for Scx^{Ai9} cell localization and collagen deposition (Fig. 6A). Although a few bridging Scx^{Ai9} cells were observed in approximately half of the day 8 repair samples, Scx^{Ai9} cells were consistently bridging by day 10 post-repair (Fig. 6B and C). A defined collagen bridge is first present at day 10 post-repair (Fig. 6C), but is not as robust as the collagen bridge present at 14 days post-repair(4). Bridging Scx^{Ai9} cells and bridging collagen matrix are both present at day 12 (Fig. 6D) and are comparable with day 14 repairs(4). Interestingly, the cells existing at the bridging collagen boundary are predominantly non-Scx^{Ai9}, suggesting a different population may be defining, and possibly producing, the collagen bridge (Fig. 6C and D, yellow arrows).

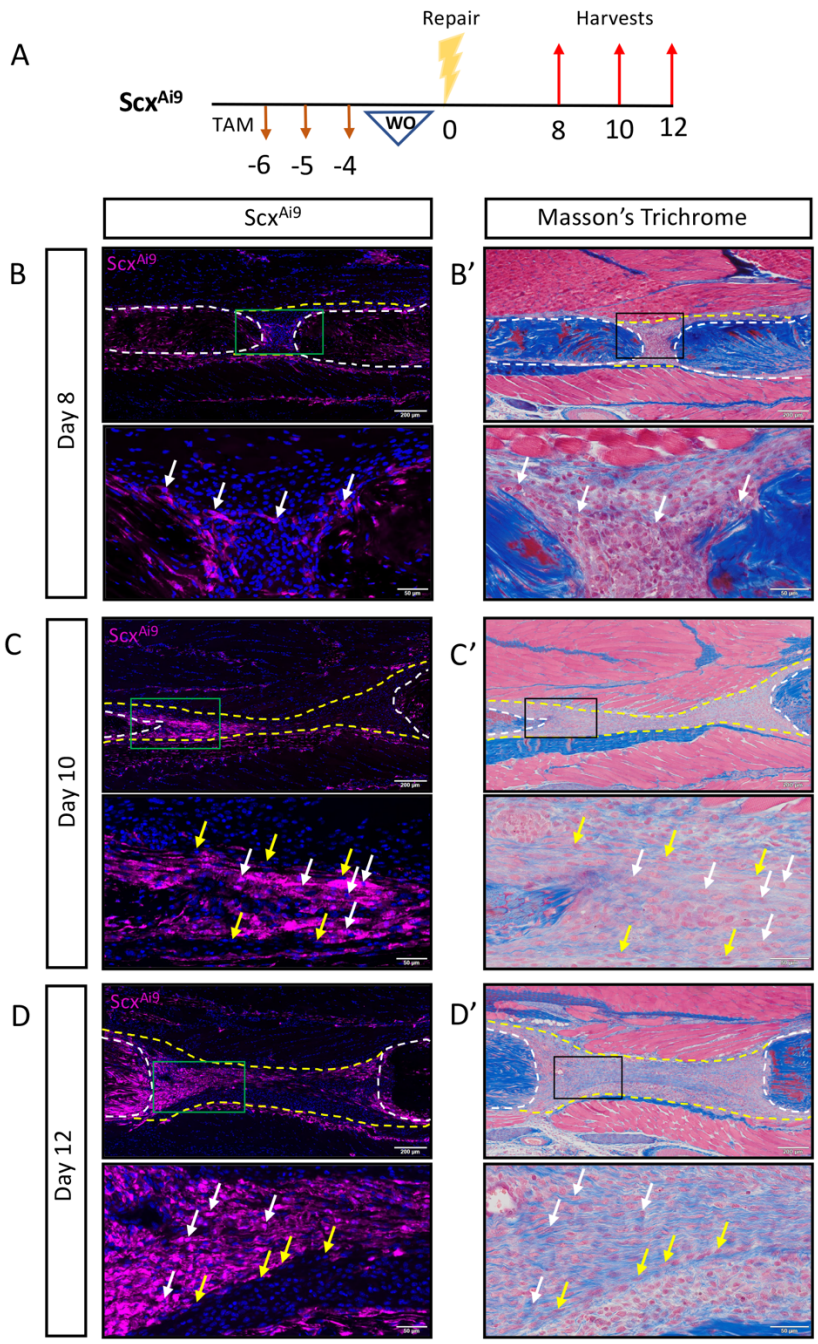

Figure 6. Bridging Scx^{Ai9} cells and bridging collagen matrix both actively form by 10 days post-repair. Scx^{Ai9} mice were injected with TAM for three days, allowed to WO for four days prior to repair surgery, and were harvested at days 8, 10, and 12 post-repair (A). Immunofluorescence of Scx^{Ai9} at days 8 (B), 10 (C), and 12 (D) post-repair. Nuclei stained with DAPI. Coverslips were removed and samples were then stained with Masson's Trichrome to analyze localization of organized collagen deposition at the repair site (B', C',D'). Tendon is outlined by white dotted lines and scar tissue by yellow dotted lines. Green and black boxes indicate location of higher magnification images. White arrows used to indicate Scx^{Ai9} cells and yellow arrows used to indicate non-Scx^{Ai9} cells between fluorescent and masson's trichrome images. N=3-4 per timepoint.

Scx^{Ai9} tendon cells proliferate at both the tendon stub and bridging tissue throughout healing.

It is unknown if bridging Scx^{Ai9} cells are derived from pre-existing Scx^{Ai9} cells that have migrated into the scar tissue space or from newly derived Scx^{Ai9} produced through proliferation that then expand into the scar. Studies examining proliferative capability of adult tendon cells during healing are limited, but most findings indicate a low proliferative ability of tendon cells during healing(11, 12, 26). To assess *in vivo* proliferative capability of Scx^{Ai9} tendon cells during flexor tendon healing, Scx^{Ai9} tendons were stained for PCNA at days 8, 10, 12, 14, 21, and 28 post-repair (Fig. 7A). While there are PCNA+ Scx^{Ai9} cells in both the tendon stub and bridging scar tissue at days 8 and 10 post-repair (Fig. 7B and C), proliferation of Scx^{Ai9} cells appeared to peak between days 12 and 14 at both the stub and bridging regions (Fig. 7D and E). While many Scx^{Ai9} cells within the stub remained PCNA+ at day 21 post-repair, bridging Scx^{Ai9} cells were almost exclusively PCNA- (Fig. 7F). By day 28 post-repair, only a few Scx^{Ai9} cells in the stub were PCNA+ and no bridging Scx^{Ai9} cells were proliferating (Fig. 7G). Therefore, bridging Scx^{Ai9} cells may be derived from both newly proliferated cells that emanate from the stub and proliferation of Scx^{Ai9} cells that have already migrated into the bridge.

Ablation of Scx^{Lin} tendon cells does not significantly affect tendon post-natal growth 3 months post-ablation.

Local injection of DT into pre-pubescent mice (3-4 weeks old) resulted in 55% depletion of tendon cells in uninjured $ScxLin^{DTR}$ FDL tendons relative to WT littermates ($p = 0.0007$) (Fig. 8A-C). To assess the requirement for tendon cells in post-natal growth, pre-pubescent mice who were still undergoing periods of rapid growth were injected with DT and harvested at the 3-month timepoint ($ScxLin^{DTR,3weeks}$) (Fig. 8D). There were no significant changes in MTP range of motion, gliding resistance, stiffness, or maximum load at failure between groups (Fig. 8E-H). Second harmonic generation revealed no significant differences in collagen fibril dispersion between genotypes (Fig. 8I and J). $ScxLin^{DTR,3weeks}$ tendons did not exhibit an influx of F4/80+ macrophages or tendon cell differentiation into αSMA+ myofibroblasts in either genotype (Fig. 8K); however,

ScxLin^{DTR} mice had a 42.5% decreased tendon cell number relative to WT littermates ($p = 0.0454$) (Fig. 8K and L).

Ablation of Scx^{Lin} tendon cells does not significantly affect tendon homeostasis 3 months post-depletion. To assess the requirement for Scx^{Lin} tendon cells in maintaining tendon homeostasis, adult (10-12 weeks) ScxLin^{DTR} mice were injected with DT to induce cell death and harvested after 3 months (ScxLin^{DTR,10weeks}) (Fig. 9A). There were no significant changes in tendon gliding function or biomechanical properties between genotypes after 3 months (Fig. 9B-E). While ScxLin^{DTR,10weeks} animals were trending towards decreased maximum load at failure relative to WT littermates, these differences did not reach significance (WT: 9.16 ± 0.57, ScxLin^{DTR,10weeks}: 7.63 ± 0.51, $p = 0.0677$) (Fig. 9E). Second harmonic generation revealed a trending increase in collagen fibril dispersion in ScxLin^{DTR,10weeks} relative to WT littermates (WT: 9.085 ± 0.72, ScxLin^{DTR,10weeks}: 11.15 ± 0.53, $p=0.0806$) (Fig. 9F and G). ScxLin^{DTR,10weeks} tendons did not exhibit an influx of F4/80+ macrophages or tendon cell differentiation into αSMA+ myofibroblasts in either genotype (Fig. 9H); however, ScxLin^{DTR} mice had a 41% decreased tendon cell number relative to WT littermates ($p = 0.0358$) (Fig. 9H and I).

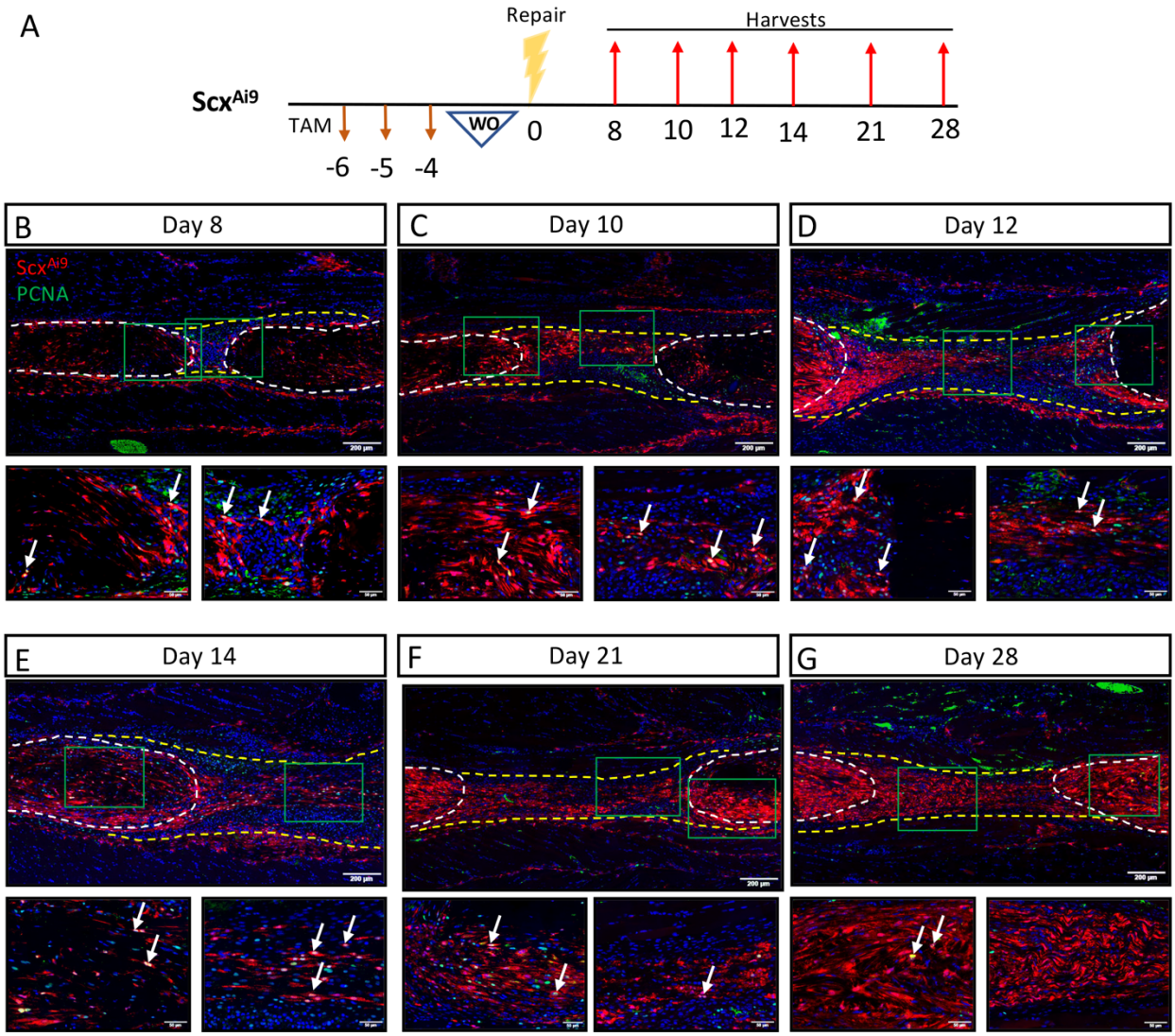

Figure 7. Scx^{Ai9} cells residing in both the tendon stubs and bridging tissue proliferate through day 21 post-repair. Scx^{Ai9} mice were injected with TAM for three days, allowed to WO for four days prior to repair surgery, and were harvested at days 8, 10, 12, 14, 21, and 28 days post-repair (A). Co-immunofluorescence of Scx^{Ai9} (red) and PCNA (green) at 8 (B), 10 (C), 12 (D), 14 (E), 21 (F), and 28 (G) days post-repair. Nuclei stained with DAPI. Tendon is outlined by white dotted lines and scar tissue by yellow dotted lines. Green boxes indicate location of higher magnification images (Left: tendon stub, Right: bridging tissue). Examples of co-localization indicated by white arrows. N=3-4 per timepoint.

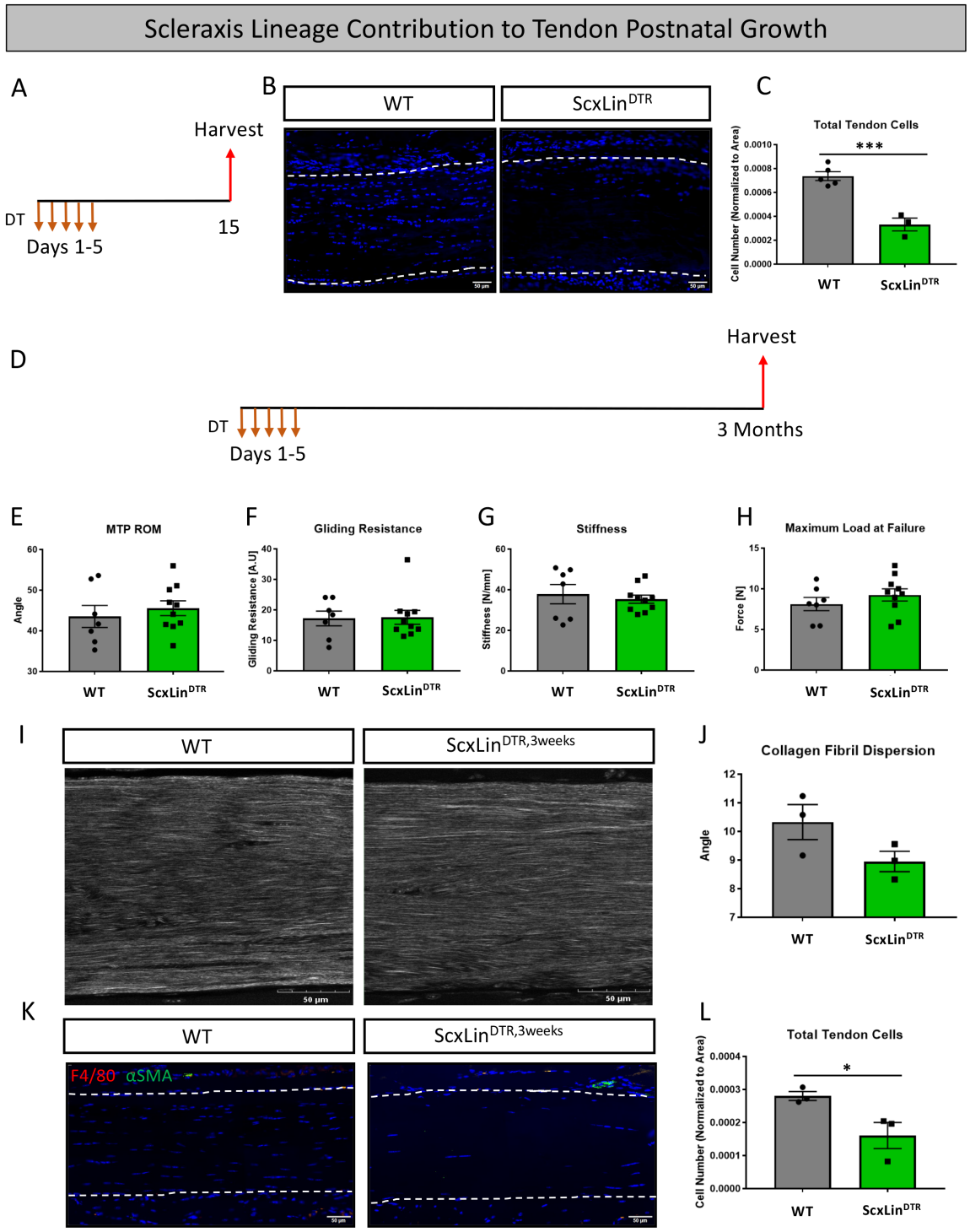

Figure 8. Tendon cell ablation does not negatively affect post-natal tendon growth 3 months post-ablation. Pre-pubescent mice (3-4 weeks old) received five hindpaw injections of DT and were harvested ten days after the final injection to assess tendon cell depletion (ScxLin^{DTR}) (A). Hindpaw sections from both WT and ScxLin^{DTR} hindpaws (B). Quantification of WT and ScxLin^{DTR,3weeks} tendon cell number in pre-pubescent mice (C). To assess effects of tendon cell depletion on post-natal tendon growth, mice received five hindpaw injections of DT on consecutive days at 3-4 weeks of age and were harvested uninjured 3 months later for biomechanical, gliding, and histological evaluation (ScxLin^{DTR,3weeks}) (D). Measurement of metatarsophalangeal (MTP) joint flexion angle (E), gliding resistance (F), stiffness (G), and maximum load at failure (H) of WT and ScxLin^{DTR,3weeks} uninjured tendons. N=7-10 per genotype. Second harmonic generation (I) and quantification (J) of collagen fibril dispersion of WT and ScxLin^{DTR,3weeks}. Co-immunofluorescence of F4/80 (macrophages) and αSMA (myofibroblasts) in uninjured WT and ScxLin^{DTR,3weeks} tendons (K). Quantification of WT and ScxLin^{DTR,3weeks} tendon cell number (L). Nuclei stained with DAPI. Tendon is outlined by white dotted lines. N=3 per genotype. For SHG, 3 sections from 3 samples per genotype were imaged and used for quantification. Student's t-test used to assess statistical significance between genotypes. * indicates $p < 0.05$, *** indicates $p < 0.001$.

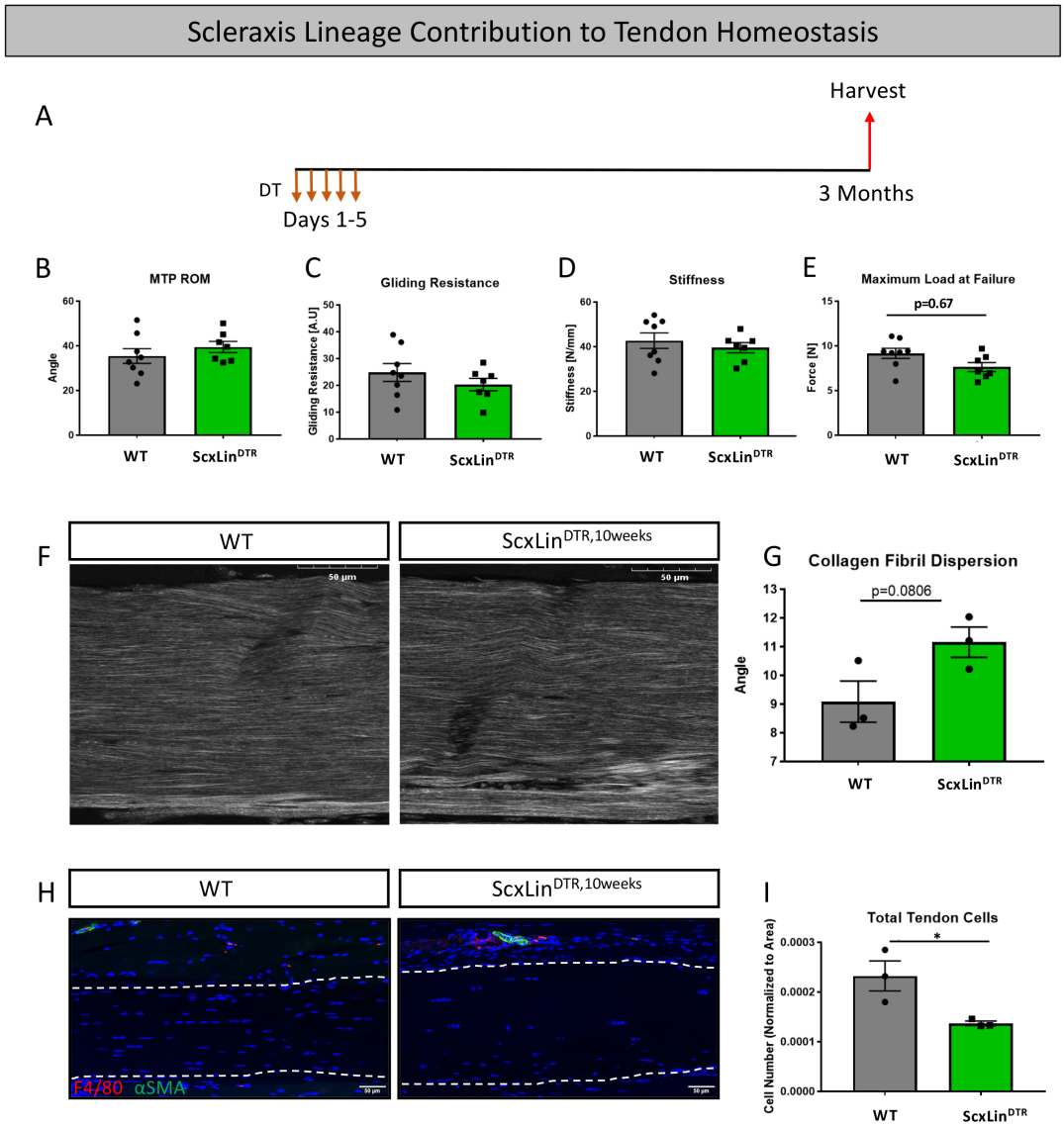

Figure 9. Tendon cell ablation does not negatively affect tendon homeostasis 3 months post-ablation. Mice received five hindpaw injections of DT on consecutive days at 10-12 weeks of age and were harvested uninjured 3 months later for biomechanical, gliding, and histological evaluation (ScxLin^{DTR,10weeks}) (A). Measurement of metatarsophalangeal (MTP) joint flexion angle (B), gliding resistance (C), stiffness (D), and maximum load at failure (E) of WT and ScxLin^{DTR,10weeks} uninjured tendons. N=7-8 per genotype. Second harmonic generation (SHG) (F) and quantification (G) of collagen fibril dispersion of WT and ScxLin^{DTR,10weeks}). Co-immunofluorescence of F4/80 (macrophages) and αSMA (myofibroblasts) in uninjured WT and ScxLin^{DTR} tendons (H). Nuclei stained with DAPI. Tendon is outlined by white dotted lines. Quantification of WT and ScxLin^{DTR,10weeks} tendon cell number (I). N=3 per genotype. For SHG, 3 sections from 3 samples per genotype were imaged and used for quantification. Student's t-test used to assess statistical significance between genotypes. * indicates $p < 0.05$.

Discussion:

In the present study we examined the function of Scx^{Lin} tendon cells during healing and made the surprising discovery that Scx^{Lin} cell depletion significantly enhanced biomechanical properties by day 28 post-repair. Additionally, we further characterized the localization, proliferative ability, and fate of Scx^{Lin} tendon cells during healing. Lastly, we examined the effects of Scx^{Lin} cell depletion on post-natal tendon growth and adult tendon homeostasis.

Tendon cell depletion had surprisingly beneficial effects on healing, with biomechanical properties significantly increased at day 28 post-repair relative to WT controls with no impact on gliding function. These results indicate that the improved biomechanical properties are not due to increased levels of matrix/scar components within the healing tendon, but that the healing process is shifted towards a regenerative phenotype. Equally striking is that the significant improvements in biomechanical properties did not emerge until 28 days post-repair, which is firmly into the remodeling phase of healing. This suggests that *Scx*^{Lin} cells are important in the late proliferative-remodeling phases of healing and possibly enact their greatest effects by modulating the remodeling process. It has previously been reported that tendon strength is still significantly decreased relative to uninjured controls 63 days post-repair using this model(27). Therefore, it could be beneficial to examine time points beyond day 28 to see if $ScxLin^{DTR}$ tendons reach equivalency with uninjured controls. The improved biomechanical properties contrasted with our original hypothesis where we predicted *Scx*^{Lin} cells would be necessary for proper healing and would contribute to formation of the bridging collagen tissue. Both $ScxLin^{DTR}$ and WT mice exhibited a collagen bridge at 14 and 28 days post-repair suggesting that Scx^{Lin} cells are not the predominant cell population laying down this collagenous matrix. This is surprising due to studies demonstrating *Scx* promotes collagen formation(11, 20), but highlights the important distinction between Scx^{Lin} cells and active *Scx* expression.

While myofibroblast persistence is considered a primary driver of fibrosis(28), recent work has revealed that myofibroblasts are a highly heterogenous population with differences in pro-fibrotic markers, gene expression, and cross-linking ability, suggesting that myofibroblasts contribute to both fibrotic and regenerative

processes(29). Despite the elevated myofibroblast presence in ScxLin^{DTR} repairs at day 28, these tendons healed with increased biomechanical properties while experiencing no deficits in tendon range of motion, suggesting a more regenerative healing process. Future work to assess the myofibroblast landscape in both WT and ScxLin^{DTR} mice is necessary to determine if ScxLin^{DTR} myofibroblasts are more "pro-regenerative" than those present in WT controls. Related to this, the cell-lineage of myofibroblast origin is also associated with function. We have previously shown that Scx^{Ai9} in the bridging collagen matrix do not become myofibroblasts at D14. Consistent with this, the bridging tendon cells remained αSMA^{-} through day 28 of healing, suggesting that bridging Scx^{Ai9} tendon cells are resistant to myofibroblast differentiation. We also demonstrated that most αSMA+ myofibroblasts are actively expressing *Scx* by day 14 post-repair, suggesting a non-Scx^{Ai9} population that differentiates into αSMA+ myofibroblasts and expresses *Scx* during healing (Fig. 5E). Developing a better understanding of distinctive stub vs bridging Scx^{Ai9} tendon cell differentiation patterns, delineating lineage-specific myofibroblast populations, and analysis of the relationship between *Scx* expression and αSMA+ myofibroblast differentiation will greatly enhance our understanding of tendon healing.

In addition to investigating the role of tendon cells during healing, we also utilized ScxLin^{DTR} mice to assess how tendon cell ablation affected post-natal growth (ScxLin^{DTR,3weeks}) and homeostasis (ScxLin^{DTR,10weeks}). Although there were no significant differences in gliding function or biomechanical properties between ScxLin^{DTR} and WT genotypes in either age group, ScxLin^{DTR,10weeks} animals were trending towards decreased maximum load at failure relative to wildtype controls 3 months following the final injection ($p = 0.0677$) while also trending towards increased collagen fibril dispersion ($p = 0.0806$). This suggested that loss of Scx^{Lin} cells may be detrimental to tendon tissue maintenance, but that negative biomechanical and organizational effects are not manifested until later than 3-months post-depletion. Future studies looking beyond the 3-month time-point will be informative to understand the role of tendon cells on maintenance of tendon tissue. It is also possible that negative effects on tendon biomechanical properties could be the result of Scx^{Lin} cell death in non-tendon tissues, such as muscle in the hindpaw(30). Despite nearly identical depletion efficiencies between ScxLin^{DTR,3weeks} and ScxLin^{DTR,10weeks} animals, only ScxLin^{DTR,10weeks} tendons were trending towards

disorganization and impaired biomechanical properties. This suggests possible differences in tendon cell sub-populations present during growth and homeostasis, as well as the potential contribution of extrinsic progenitor populations to tendon growth(13), such that depletion could differentially impact post-natal growth and adult tendon homeostasis.

Initial plans to deplete tendon cells using the inducible Scx-Cre^{ERT2} crossed to the diphtheria toxin A mouse(31), but insufficient recombination occurred and targeted cell death was not achieved. Therefore, to successfully deplete tendon cells Scx-Cre mice were crossed to a diphtheria toxin receptor mouse model (ScxLin^{DTR})(32). The initial attempt to deplete cells using this model employed a series of intraperitoneal injections (200ng/day) and resulted in all ScxLin^{DTR} mice dying within four days of the initial injection while WT animals were unaffected. ScxLin^{DTR} mice likely died due to apoptosis of non-tendon/ligament associated Scx^{Lin} cells. For example, it has previously been shown that *Scx* is expressed in the lung(23, 33), kidney(23), muscle(30), and brain,(33) among others. Therefore, to successfully utilize this model of cell depletion while simultaneously preventing ScxLin^{DTR} associated mouse death, a series of low-dose (20 ng/day) local hindpaw injections were administered. We successfully utilized this model of *in vivo* tendon cell depletion and reached a depletion level of 57%. Therefore, the ScxLin^{DTR} data should be viewed as a model of partial depletion as ~40% of tendon cells remained using this approach. Future work utilizing increased or prolonged DT treatment could be attempted to obtain more complete tendon cell depletion. The beneficial effects of tendon cell depletion may be reversed with complete ablation of Scx^{Lin} cells from the tendon. Additionally, our current ScxLin^{DTR} ablation model targets cells prior to injury and thus does not target any cells that turn on *Scx* after injury. It has previously been shown that *Scx* knockout during Achilles tendon healing drives incomplete remodeling of type III collagen to type I collagen(11). It could be interesting to assess if depletion of cells actively expressing *Scx* during healing resulted in deleterious effects on healing. However, local DT injection into the hindpaw following repair surgery would likely be difficult as the repair site could easily be disturbed.

Altogether, these data demonstrate that Scx^{Lin} cell depletion is beneficial for tendon healing as it increases biomechanical properties such as maximum load at failure several weeks after repair, and this may be

due to an αSMA+ myofibroblast-mediated mechanism. Furthermore, bridging Scx^{Ai9} cells do not differentiate into αSMA+ myofibroblasts following FDL injury and repair, but do readily proliferate and have a clear relationship with bridging collagen in the scar. Lastly, Scx^{Lin} depletion does not significantly disrupt tendon post-natal growth or homeostasis by 3 months post-repair; however, these data suggest that homeostasis may be disrupted in the long-term following depletion. Understanding the complex nature of tendon cells during healing, growth, and homeostasis can provide us with insights for driving regenerative healing and healthy tendon maintenance in the future.

Methods:

Mice

Scx-Cre^{ERT2} and Scx-Cre mice were generously provided by Dr. Ronen Schweitzer. C57Bl/6J (#000664), ROSA-Ai9$^{F/F}$ (#007909), and DTR$^{F/F}$ (#007900) mice were obtained from the Jackson Laboratory (Bar Harbor, ME, USA). ROSA-Ai9$^{F/F}$ mice express Tomato red fluorescence in the presence of Cre-mediated recombination(34). Scx-Cre^{ERT2} mice were crossed to the ROSA-Ai9$^{F/F}$ reporter mouse to trace adult *Scx*+ tendon cells. To induce fluorescence in *Scx*+ tendon cells prior to repair surgery, Scx-Cre^{ERT2}; ROSA-Ai9$^{F/F}$ mice received three tamoxifen injections (100 mg/kg, intraperitoneal) starting six days prior to repair surgery, allowing for a four-day washout period as previously described (Scx^{Ai9})(4). To label cells that are expressing *Scx* during the proliferative phase of healing, Scx-Cre^{ERT2}; ROSA-Ai9$^{F/F}$ received tamoxifen injections on days 10-12 post-repair (Scx$^{10-12}$). Scx-Cre mice were crossed to ROSA-Ai9$^{F/F}$ mice to label *Scx* lineage cells (Scx^{Lin}). Diphtheria toxin receptor (DTR$^{F/F}$) mice can be utilized to temporally ablate cell populations driven by a non-inducible Cre driver(32). In short, diphtheria toxin receptors are present on cells expressing Cre such that administration of diphtheria toxin (DT) to these mice results in targeted cell death. Scx-Cre mice were crossed to DTR$^{F/F}$ animals to generate a model of Scx^{Lin} tendon cell depletion (ScxLin^{DTR}) and Cre- wildtype littermates (WT). All mouse studies were performed with 10-12 week-old male and female mice except where otherwise noted (Figure 10, 3-4 week old male and female mice).

Flexor Tendon Repair

Complete transection and repair of the murine flexor digitorum longus (FDL) tendon was performed as previously described(35). Mice received a 15-20µg injection of sustained-release buprenorphine. Mice were anesthetized with Ketamine (60mg/kg) and Xylazine (4mg/kg). To reduce chances of rupture at the repair site, the FDL tendon was first transected at the myotendinous junction and the skin was closed with a 5-0 suture. Next, a small incision was made to the posterior surface of the right hindpaw, the FDL tendon was isolated from surrounding tissue and completely transected. The tendon was repaired using 8-0 suture and the skin was closed

with a 5-0 suture. Animals resumed prior cage activity, food intake, and water consumption immediately following surgery.

Quantification of Tendon Cell Depletion and Scx^{Lin} Cells

$ScxLin^{DTR}$ mice were injected with 20ng of diphtheria toxin (DT) for five consecutive days (100ng total DT). Uninjured hindpaws were harvested 10 days after the final injection for frozen sectioning. Scx^{Lin} hindpaws were harvested uninjured. Hindpaws were fixed in 10% NBF for 24 hours, decalcified in 14% EDTA for four days, and processed in 30% sucrose to cryo-protect the tissue. Samples were embedded using Cryomatrix (Thermo Fisher Scientific, Waltham, MA, USA) and sectioned into 8 mm sagittal sections using an established cryotape-transfer method(36). Sections were stained with DAPI to visualize nuclei and imaged using a VS120 Virtual Slide Microscope (Olympus, Waltham, MA). Using Image J, a ROI was drawn around the tendon and an area was obtained. For $ScxLin^{DTR}$ and WT littermate mice, nuclei within the ROI were manually counted and total nuclei number was normalized to area. For Scx^{Lin} mice, fluorescent cells in uninjured sections were manually counted and Scx^{Lin+} cells reported as a percentage of total cells counted in each section. An n = 3-4 was used for quantification.

Paraffin Histology and Immunofluorescence

Hindpaws from Scx^{Ai9} mice were harvested at days 8, 10, 12, 14, 21, and 28 post-repair and Scx^{10-12} harvested at day 14. $ScxLin^{DTR}$ hindpaws were harvested uninjured 10-days following the final DT injection and at 14- and 28-days post-repair. Additionally, $ScxLin^{DTR}$ hindpaws from adult (10-12 weeks) and pre-pubescent (3-4 weeks) mice were harvested uninjured 3 months following the final DT injection to assess effects of tendon cell depletion on tendon homeostasis. Hindpaws were fixed in 10% neutral buffered formalin (NBF) at room temperature for 72 hours and were subsequently decalcified in Webb Jee EDTA (pH 7.2-7.4) for 7 days at room temperature, processed, and embedded in paraffin. Three-micron sagittal sections were utilized for analysis, except for the 3-month study which were cut at 5-micron to facilitate SHG imaging. $ScxLin^{DTR}$ repair sections

were stained with Alcian blue/hematoxylin and Orange G (ABHOG) to assess tissue morphology and Masson's Trichrome to assess collagen deposition. For immunofluorescent staining, sections were stained with Cleaved Caspase 3 (1:100, Cat#: 9661, Cell Signaling, Danvers, MA), PCNA (1:100, Cat#:ab29, Abcam, Cambridge, MA), F4/80 (1:500, Cat#: sc-26643, Santa Cruz, Dallas, TX), α-SMA-CY3 (1:200, Cat#: C6198, Sigma Life Sciences, St. Louis, MO), α-SMA-FITC (1:500, Cat#: F3777, Sigma Life Sciences, St. Louis, MO), S100a4 (1:2000, Cat#: ab197896, Abcam, Cambridge, MA), or tdTomato (1:500, Cat#: AB8181, SICGEN, Cantanhede, Portugal). Sections were counterstained with the nuclear DAPI stain and imaged with a VS120 Virtual Slide Microscope (Olympus, Waltham, MA). Following initial imaging of the Scx^{Ai9} day 8, 10, and 12 sections, coverslips were carefully removed in PBS and subsequently stained with Masson's Trichrome.

Quantification of Fluorescence

Fluorescent images scanned by the virtual slide scanner were quantified using Visiopharm image analysis software v.6.7.0.2590 (Visiopharm, Hørsholm, Denmark). Automatic segmentation via a threshold classifier was utilized to define and quantify specific cell populations based on fluorescence. A region of interest (ROI) was drawn to encapsulate both the scar tissue and tendon stubs. The area of fluorescent signal was determined and normalized to the total ROI area to determine percentages of each cell type. An n = 4 was used for quantification.

Quantitative Assessment of Gliding Function and Biomechanical Properties

Gliding function of uninjured and repaired $ScxLin^{DTR}$ tendons was assessed as previously described(37). Hindlimbs were harvested at the knee-joint and the FDL tendon was disconnected at the myotendinous junction. The FDL tendon was secured between two pieces of tape using superglue and the tendon was loaded incrementally with small weights ranging from 0 to 19g. Images were captured unloaded and after each load and measurements of the flexion angle of the metatarsophalangeal (MTP) joint were made using Image J. Gliding resistance was derived from the changes in MTP flexion angle over the range of applied loads. An

increase in Gliding Resistance and decrease in MTP Flexion Angle is associated with restricted range of motion and increased scar tissue. After conclusion of gliding testing, the FDL tendon was released from the tarsal tunnel while the proximal end of the tendon and the toes of the hindpaw were secured into an Instron 8841 uniaxial testing system (Instron Corporation, Norwood, MA). The tendon was loaded until failure at a rate of 30mm/minute. Seven-12 samples per genotype per time-point were assessed.

Second Harmonic Generation 2-Photon Confocal Imaging

Five-micron sections of ScxLin^{DTR} hindpaws were utilized for second harmonic generation (SHG) imaging. Sections were scanned with a Spectra-Physics MaiTai HP DeepSee Ti:Sapphire Laser, tuned to 1000nm, under 25x magnification, with a 2.5X optical zoom, with a step size of 0.25µm. 3D projections of image stacks were generated using the 3D-Project macro in ImageJ and analyzed for collagen fibril uniformity using the Directionality macro. The Directionality macro utilizes Fourier transform analysis to derive spatial orientation of image stacks. Three tissue sections from 3 samples per genotype per age group were used to quantify collagen fibril dispersion. Each data point on the graph is representative of averaged dispersion across three sections. N=3 per genotype per age group, and N=3 sections per sample.

Statistics

Quantitative data was analyzed via GraphPad Prism and is presented as mean $\pm$ standard error of the mean (SEM). Either a student's t-test or two-way analysis of variance (ANOVA) with Sidak's multiple comparisons test was used to analyze data when data was normal. A Mann-Whitney test was utilized when data was not distributed normally (D28 F4/80 and S100a4 immunofluorescence, figure 4). p values ≤ 0.05 were considered significant. * indicates $p<0.05$, ** indicates $p<0.01$, *** indicates $p<0.001$, **** indicates $p<0.0001$.

Study Approval

This study was carried out in strict accordance with the recommendations in the Guide for the Care and Use of Laboratory Animals of the National Institutes of Health. All animal procedures described were approved by the University Committee on Animal Research (UCAR) at the University of Rochester Medical Center.

Author contributions: Study conception and design: KTB, AEL; Acquisition of data: KTB, KMM, EK; Analysis and interpretation of data: KTB, MRB, AEL; Drafting of manuscript: KTB, AEL; Revision and approval of manuscript: KTB, KMM, EK, MRB, AEL.

Acknowledgements: We would like to thank the Histology, Biochemistry and Molecular Imaging (HBMI) and the Biomechanics, Biomaterials and Multimodal Tissue Imaging (BBMTI) for technical assistance with the histology and biomechanical testing, respectively. We would also like to thank the Multiphoton & Analytical Imaging Center (MAGIC) at URMC for assistance with Second Harmonic Generation Imaging.

Funding: This work was supported in part by NIH/ NIAMS F31 AR074815 (to KTB), K01AR068386 and R01AR073169 (to AEL) and R01AR070765 (to MRB). The HBMI and BBMTI Cores were supported by NIH/ NIAMS P30AR069655. The content is solely the responsibility of the authors and does not necessarily represent the official views of the National Institutes of Health.

Competing Interests: The authors declare no competing interests.

Data Availability Statement: All data generated or analyzed during this study are included in this article.

References

1. Nichols AEC, Best KT, and Loiselle AE. The cellular basis of fibrotic tendon healing: challenges and opportunities. *Translational research : the journal of laboratory and clinical medicine.* 2019;209:156-68.
2. Walia B, and Huang AH. Tendon stem progenitor cells: Understanding the biology to inform therapeutic strategies for tendon repair. *J Orthop Res.* 2019;37(6):1270-80.
3. Costa-Almeida R, Calejo I, and Gomes ME. Mesenchymal Stem Cells Empowering Tendon Regenerative Therapies. *International journal of molecular sciences.* 2019;20(12).
4. Best KT, and Loiselle AE. Scleraxis lineage cells contribute to organized bridging tissue during tendon healing and identify a subpopulation of resident tendon cells. *FASEB journal : official publication of the Federation of American Societies for Experimental Biology.* 2019:fj201900130RR.
5. Swanson JB, Micheli AJD, Disser NP, Martinez LM, Walker NR, Cosgrove BD, et al. A single-cell transcriptional atlas identifies extensive heterogeneity in the cellular composition of tendons. *bioRxiv.* 2019:801266.
6. Kendal A, Layton T, Al-Mossawi H, Brown R, Loizou C, Rogers M, et al. Identification of human tendon cell populations in healthy and diseased tissue using combined single cell transcriptomics and proteomics. *bioRxiv.* 2019:2019.12.09.869933.
7. Schweitzer R, Chyung JH, Murtaugh LC, Brent AE, Rosen V, Olson EN, et al. Analysis of the tendon cell fate using Scleraxis, a specific marker for tendons and ligaments. *Development.* 2001;128(19):3855-66.
8. Murchison ND, Price BA, Conner DA, Keene DR, Olson EN, Tabin CJ, et al. Regulation of tendon differentiation by scleraxis distinguishes force-transmitting tendons from muscle-anchoring tendons. *Development (Cambridge, England).* 2007;134(14):2697-708.

9. Pryce BA, Watson SS, Murchison ND, Staverosky JA, Dunker N, and Schweitzer R. Recruitment and maintenance of tendon progenitors by TGFbeta signaling are essential for tendon formation. *Development (Cambridge, England).* 2009;136(8):1351-61.

10. Huang AH, Watson SS, Wang L, Baker BM, Akiyama H, Brigande JV, et al. Requirement for scleraxis in the recruitment of mesenchymal progenitors during embryonic tendon elongation. *Development.* 2019;146(20).

11. Sakabe T, Sakai K, Maeda T, Sunaga A, Furuta N, Schweitzer R, et al. Transcription factor scleraxis vitally contributes to progenitor lineage direction in wound healing of adult tendon in mice. *J Biol Chem.* 2018;293(16):5766-80.

12. Howell K, Chien C, Bell R, Laudier D, Tufa SF, Keene DR, et al. Novel Model of Tendon Regeneration Reveals Distinct Cell Mechanisms Underlying Regenerative and Fibrotic Tendon Healing. *Scientific reports.* 2017;7:45238.

13. Dyment NA, Hagiwara Y, Matthews BG, Li Y, Kalajzic I, and Rowe DW. Lineage tracing of resident tendon progenitor cells during growth and natural healing. *PloS one.* 2014;9(4):e96113.

14. Bavin EP, Atkinson F, Barsby T, and Guest DJ. Scleraxis Is Essential for Tendon Differentiation by Equine Embryonic Stem Cells and in Equine Fetal Tenocytes. *Stem cells and development.* 2017.

15. Chen X, Yin Z, Chen JL, Shen WL, Liu HH, Tang QM, et al. Force and scleraxis synergistically promote the commitment of human ES cells derived MSCs to tenocytes. *Scientific reports.* 2012;2:977.

16. Alberton P, Popov C, Pragert M, Kohler J, Shukunami C, Schieker M, et al. Conversion of human bone marrow-derived mesenchymal stem cells into tendon progenitor cells by ectopic expression of scleraxis. *Stem Cells Dev.* 2012;21(6):846-58.

17. Nichols AC, Werre SR, and Dahlgren LA. Transient scleraxis overexpression combined with cyclic strain enhances ligamentous differentiation. *Tissue engineering Part A.* 2018.

18. Maeda T, Sakabe T, Sunaga A, Sakai K, Rivera AL, Keene DR, et al. Conversion of mechanical force into TGF-beta-mediated biochemical signals. *Current biology : CB.* 2011;21(11):933-41.

19. Nichols AEC, Settlage RE, Werre SR, and Dahlgren LA. Novel roles for scleraxis in regulating adult tenocyte function. *BMC Cell Biol.* 2018;19(1):14.

20. Lejard V, Brideau G, Blais F, Salingcarnboriboon R, Wagner G, Roehrl MH, et al. Scleraxis and NFATc regulate the expression of the pro-alpha1(I) collagen gene in tendon fibroblasts. *The Journal of biological chemistry.* 2007;282(24):17665-75.

21. Levay AK, Peacock JD, Lu Y, Koch M, Hinton RB, Jr., Kadler KE, et al. Scleraxis is required for cell lineage differentiation and extracellular matrix remodeling during murine heart valve formation in vivo. *Circulation research.* 2008;103(9):948-56.

22. Al-Hattab DS, Safi HA, Nagalingam RS, Bagchi RA, Stecy MT, and Czubryt MP. Scleraxis regulates Twist1 and Snai1 expression in epithelial-to-mesenchymal transition. *American journal of physiology Heart and circulatory physiology.* 2018.

23. Pryce BA, Brent AE, Murchison ND, Tabin CJ, and Schweitzer R. Generation of transgenic tendon reporters, ScxGFP and ScxAP, using regulatory elements of the scleraxis gene. *Dev Dyn.* 2007;236(6):1677-82.

24. Best KT, Lee FK, Knapp E, Awad HA, and Loiselle AE. Deletion of NFKB1 enhances canonical NF-κB signaling and increases macrophage and myofibroblast content during tendon healing. *Scientific reports.* 2019;9(1):10926.

25. Ackerman JE, Nichols AE, Studentsova V, Best KT, Knapp E, and Loiselle AE. Cell non-autonomous functions of S100a4 drive fibrotic tendon healing. *Elife.* 2019;8.

26. Dyment NA, Liu CF, Kazemi N, Aschbacher-Smith LE, Kenter K, Breidenbach AP, et al. The paratenon contributes to scleraxis-expressing cells during patellar tendon healing. *PloS one.* 2013;8(3):e59944.

27. Loiselle AE, Bragdon GA, Jacobson JA, Hasslund S, Cortes ZE, Schwarz EM, et al. Remodeling of murine intrasynovial tendon adhesions following injury: MMP and neotendon gene expression. *Journal of orthopaedic research : official publication of the Orthopaedic Research Society.* 2009;27(6):833-40.

28. Hinz B, and Lagares D. Evasion of apoptosis by myofibroblasts: a hallmark of fibrotic diseases. *Nature reviews Rheumatology.* 2020;16(1):11-31.

29. Shook BA, Wasko RR, Rivera-Gonzalez GC, Salazar-Gatzimas E, Lopez-Giraldez F, Dash BC, et al. Myofibroblast proliferation and heterogeneity are supported by macrophages during skin repair. *Science.* 2018;362(6417).

30. Mendias CL, Gumucio JP, Davis ME, Bromley CW, Davis CS, and Brooks SV. Transforming growth factor-beta induces skeletal muscle atrophy and fibrosis through the induction of atrogin-1 and scleraxis. *Muscle & nerve.* 2012;45(1):55-9.

31. Voehringer D, Liang HE, and Locksley RM. Homeostasis and effector function of lymphopenia-induced "memory-like" T cells in constitutively T cell-depleted mice. *J Immunol.* 2008;180(7):4742-53.

32. Buch T, Heppner FL, Tertilt C, Heinen TJ, Kremer M, Wunderlich FT, et al. A Cre-inducible diphtheria toxin receptor mediates cell lineage ablation after toxin administration. *Nature methods.* 2005;2(6):419-26.

33. Perez AV, Perrine M, Brainard N, and Vogel KG. Scleraxis (Scx) directs lacZ expression in tendon of transgenic mice. *Mech Dev.* 2003;120(10):1153-63.

34. Madisen L, Zwingman TA, Sunkin SM, Oh SW, Zariwala HA, Gu H, et al. A robust and high-throughput Cre reporting and characterization system for the whole mouse brain. *Nat Neurosci.* 2010;13(1):133-40.

35. Ackerman JE, and Loiselle AE. Murine Flexor Tendon Injury and Repair Surgery. *Journal of visualized experiments : JoVE.* 2016(115).

36. Dyment NA, Jiang X, Chen L, Hong SH, Adams DJ, Ackert-Bicknell C, et al. High-Throughput, Multi-Image Cryohistology of Mineralized Tissues. *Journal of visualized experiments : JoVE.* 2016(115).

37. Hasslund S, Jacobson JA, Dadali T, Basile P, Ulrich-Vinther M, Soballe K, et al. Adhesions in a murine flexor tendon graft model: Autograft versus allograft reconstruction. *J Orthop Res.* 2008;26(6):824-33.